ARTICLES

Chemical and Transport Processes of Photoelectrons Generated in Rubidium−Tetrahydrofuran Solutions

Yehuda Heimlich,* Vladimir Rozenshtein, and Haim Levanon

Department of Physical Chemistry and the Farkas Center for Light-Induced Processes, The Hebrew University of Jerusalem, Jerusalem 91904, Israel

Leonid Lukin

Institute for Energy Problems in Chemical Physics, Russian Academy of Sciences, Chernogolovka, Moscow 142432, Russian Federation

Received: July 21, 1998; In Final Form: December 19, 1998

The mobility of photoelectrons (μ_e) was determined by measuring the transient photocurrent induced by electron photodetachment from rubidium anions (Rb^-) in liquid tetrahydrofuran (THF) in the temperature range of 180−296 K. Electrons were generated by photoexcitation of Rb/THF solutions by 532 nm laser pulses. The measured transients consisted of a fast component (~1 μs) followed by a slow decay (~10−100 μs). Negative photocurrent was observed at high temperatures and large concentrations of the Rb ions. This unusual behavior is interpreted by taking into account the recombination and dissociation reactions involving the photoelectrons (e^-) and rubidium ions (Rb^+ and Rb^-). The equilibrium constant of electron−cation dissociation was found to increase by an order of magnitude upon cooling the Rb/THF solution from 296 to 198 K. The mobility of the photoelectrons was found to be associated with an activation energy of 5.9 kJ mol^{-1}.

I. Introduction

The transport and reactivity of electrons and ions in liquids are basic problems related to radiation chemistry and photochemistry.[1] Solutions of alkali metals (M) dissolved in ethers are of particular interest since they are also related to the growing interest in quantum and spin electronics.[2,3] Kinetics of excess electrons were studied in polar liquids, e.g., water and ammonia,[1e] and in nonpolar liquids, e.g., liquefied rare gases and liquid hydrocarbons.[1b,4] As shown in these studies, the behavior of excess electrons is determined by the efficiency of electron localization, which depends on the conduction band energy of the electron in liquids, short-range electron−solvent interactions, the shape of solvent molecules, dielectric constants, and other inherent properties of the solvent. Excess electrons in liquids of intermediate permeativity, such as ethers and amines (dielectric constants, $\epsilon \approx 10$), were also investigated.[5] However, the kinetic data available (particularly for the mobility) are scarce and not fully understood. Specifically, values of the electron mobility span from 1000 $cm^2\ V^{-1}\ s^{-1}$ in liquid Kr, 500 $cm^2\ V^{-1}\ s^{-1}$ in CH_4, down to 10^{-4} $cm^2\ V^{-1}\ s^{-1}$ in C_2H_5-OH.[6]

In addition to the electron properties, the dynamics of spin-polarized electrons generated in photoexcited alkali-metal/tetrahydrofuran (M/THF) solutions were investigated.[7] In a recent EPR study of Rb^- dissolved in THF, we have reported on a parabolic dependence of the spin-relaxation rates of the photodetached electrons upon photon energy.[3] Analysis of the results led us to estimate indirectly a relatively high mobility of the photoelectrons in this system (0.1 $cm^2\ V^{-1}\ s^{-1}$ at 180 K), which is substantially different from that measured in an early study at room temperature (0.003 $cm^2\ V^{-1}\ s^{-1}$).[8]

The present study is intended to determine directly the mobility of electrons and ions and to study the reactions in photoexcited Rb/THF solutions at different temperatures. Our experimental approach is based on studying the photocurrent transients attributed to the photodetached electron from Rb^-. The quantitative analysis of the results is based upon the following reactions:[5,7,9,10−12]

$$(Rb^+, Rb^-) \underset{k_{-1}}{\overset{k_1}{\rightleftharpoons}} Rb^+ + Rb^- \quad (1)$$

$$Rb^- \underset{k_{-2}}{\overset{k_2}{\rightleftharpoons}} Rb^\bullet + e^- \quad (2)$$

$$Rb^\bullet \underset{k_{-3}}{\overset{k_3}{\rightleftharpoons}} Rb^+ + e^- \quad (3)$$

$$Rb^- + h\nu \xrightarrow{\sigma_p} Rb^\bullet + e^- \quad (4)$$

$$Rb^\bullet + Rb^\bullet \xrightarrow{k_5} Rb^+ + Rb^- \quad (5)$$

where k_i and k_{-i} are the appropriate rate constants and σ_p is the cross-section of the electron photodetachment. In this study we shall confirm the reaction steps 1−5 and quantify the kinetic mechanism associated with photoexcited Rb/THF solutions.

II. Experimental Section

THF (Aldrich Chemicals) was purified over a Na/K alloy and degassed by freeze−pump−thaw cycles. THF was distilled

10.1021/jp983094w CCC: $18.00
Published on Web 04/02/1999

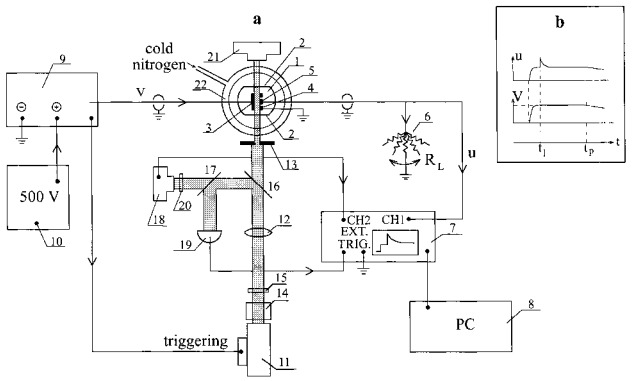

Figure 1. Schematic diagram of the experimental setup (a). Time dependence of the applied voltage, *V*, and the detected signal, *u* (b).

into the photoconductivity cell containing rubidium mirror and sealed under vacuum (10^{-5} Torr). Metal dissolution, i.e., $2Rb_{(solid)} \rightleftarrows Rb^- + Rb^+$ and $Rb_{(solid)} \rightleftarrows Rb^+ + e^-$, was carried out in a separate compartment through contact of the solvent with the mirror. After the solution was disconnected from the mirror, reactions 1−5 are the relevant ones in this study. The absolute concentration of rubidium ions was controlled by the time of contact between the solvent and the mirror. In all experiments, before metal dissolution the specific conductivity of the pure solvent was measured (10^{-7} Ω^{-1} m^{-1}). The photoconductivity was determined with the setup schematically shown in Figure 1a. The cell (1) made of Pyrex glass contained two flat optical windows (2) and three electrodes made of a platinum foil (3−5). The transient voltage drop, *u*, across a load resistance, R_L (0.2−7.5 kΩ), was measured by digitizing (Tektronix, TDS 220 (7)) the signal from the collector electrode (5). The obtained data were stored on a PC (8). The response time of the electric circuit was controlled by the known capacitance of the cable connecting the cell and the oscilloscope (∼60 pF) and was found to be 20 ns for $R_L = 0.2$ kΩ.

To escape irreversible changes in the solution and to avoid gradients of ion concentrations under the electric field, the voltage pulse, *V* (a few ms duration), was applied to the high-voltage electrode (3). This pulse (Figure 1b) with a rise time of 10−20 μs reached its maximum value ($V_0 = 400-500$ V) and decayed with a characteristic time of 5 ms at $t \geq t_p$ ($t_p \approx 0.6$ ms). The duration of the voltage pulse ($t_p - t_1$) was chosen to be much longer than any transient process due to the light excitation at t_1 and was shown as the spike on trace *u* in Figure 1b.

The light pulse (1−50 mJ/pulse, 12 ns duration, 532 nm wavelength) of the Nd:YAG laser (11) (Quanta-Ray, DCR-1A with the amplifier PDL-1) illuminated the interelectrode space along the larger side of the collector electrode. The time delay between the onset of the voltage pulse and the laser pulse was varied within a period of 0.6 ms, so that the photogenerated charge carriers were subjected only to a constant electric field, $E_0 = V_0/d$, where *d* is the separation between the electrodes (0.003 m). The cross-section area of the laser beam was confined by the diaphragm (13) with the aperture $S = 9 \times 10^{-6}$ m^2. Care was taken that the diaphragm dimension coincided with *d* and that the lens (12) focal length was much longer (1 m) than the length of the collector electrode (0.009 m). Thus, the laser beam homogeneously filled the interelectrode volume, $\Delta v = Ad \approx 10^{-7}$ m^3, where $A = 2.7 \times 10^{-5}$ m^2 is the geometrical area of the collector electrode. Passing the laser beam through an aqueous solution of $CuSO_4$ (14) and a glass filter (15) (Schott KG3) eliminated IR and UV overtones of irradiation. Using the beam splitters (16 and 17) the light was directed to the phototube

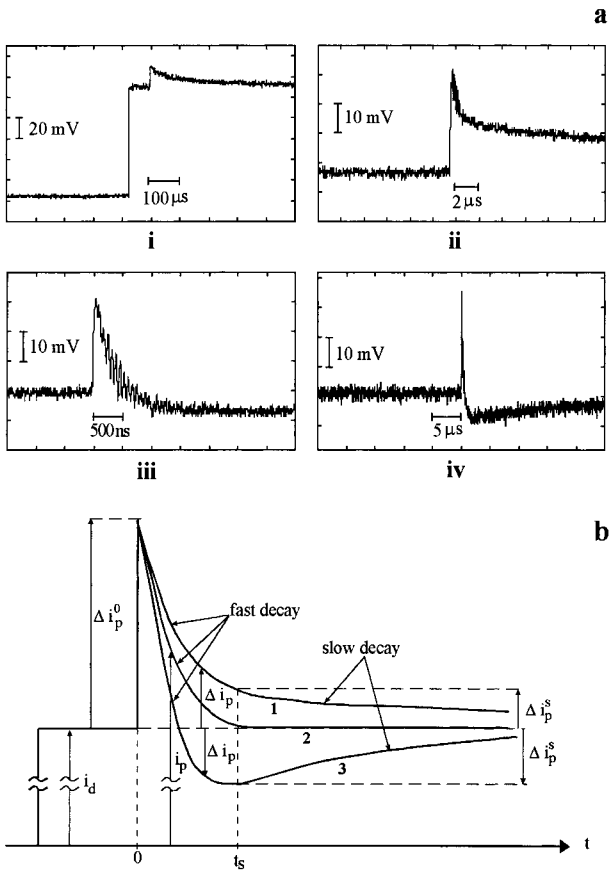

Figure 2. Experimental current traces for $n_0 = 4.2 \times 10^{-6}$ kmol m^{-3}, $E_0 = 1.53 \times 10^5$ V m^{-1}, and $W = 7.2$ mJ at different conditions: $T =$ 198 and 223 K, $R_L = 560$ Ω, i and ii, respectively; $T =$ 273 and 300 K, $R_L = 200$ Ω, iii and iv, respectively (a). Schematic description of the transient currents, following the laser pulse at $t = 0$, at different temperatures and/or [Rb^-]: low, intermediate, and high, respectively (b).

(18) (RCA I P39) to measure the laser pulse energy and to the triggering photodiode (19). The phototube response was kept in the linear regime by neutral filters (20) and calibrated by a power meter (21) (Ophir DGX-PP). All experiments were carried out in the single-pulse mode to achieve equilibrated concentrations between the successive light pulses.

Each experiment was carried out using solutions with concentrations of the Rb^- ions in the range between 2×10^{-8} (colorless) and 8×10^{-6} kmol m^{-3} (blue). Concentrations in the range of 10^{-6} kmol m^{-3} were measured by absorption spectroscopy, while lower concentrations were estimated from the dark current. The Rb^- concentration was determined using the extinction coefficients of Rb^- at 800 and 500 nm ($\epsilon_{800} - \epsilon_{500} = 5.4 \times 10^6$ m^2 $kmol^{-1}$).[9] It should be noted that under dark conditions, no EPR signals due to the electrons or radicals could be detected, even in the saturated solution (8×10^{-6} kmol m^{-3}). This provides an upper limit to the dark electrons in thermal equilibrium, $[e^-]_{eq} < 10^{-8}$ kmol m^{-3}.[7c] Temperatures between 170 and 300 K were maintained by a temperature controller (Eurotherm 808) in a glass dewar (22).

III. Results

III.1. Kinetic Data. Typical experimental traces of the voltage taken at various temperatures are presented in Figure 2a. The different parameters associated with each trace are shown in Figure 2b. For a coherent presentation, trace i in Figure 2a also shows the initial voltage response (dark current). The

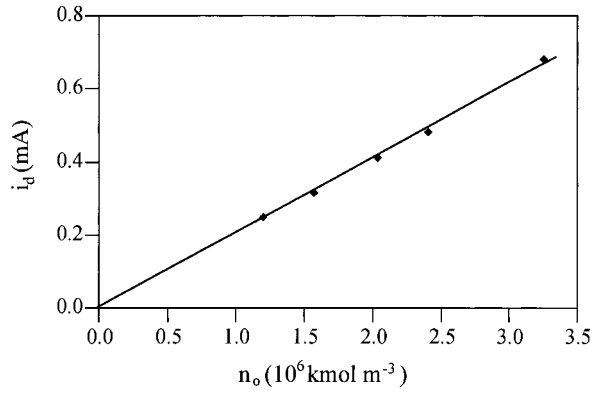

Figure 3. Amplitude of the dark current, i_d, vs n_0 at $T = 296$ K and $V_0 = 460$ V.

time for switching the laser on was chosen such that the induced photocurrent and its decay should occur while the electric field, E_0, was kept constant. This ensures that the dark current will not change before and after the laser pulse, i.e., during a few hundreds of microseconds. Thus, the photocurrent, Δi_p, can be obtained by subtracting the dark current, i_d, from the total detected current, i_p (Figure 2b).

III.2. Dark Current. The dark current i_d (u_d/R_L) was determined by the dark voltage signal, u_d, and the resistance, R_L, and was kept proportional to V_0. Under equilibrium, the dark current depends on the fields and species surrounding the collector electrode and is expressed by

$$i_d = \kappa \int \vec{E} d\vec{s} = \kappa E_0 A_{eff} \tag{6}$$

where the integration is over a surface surrounding the collector electrode, $\vec{E}$ is the electric field on this surface, $A_{eff} = E_0^{-1} \int \vec{E}\, d\vec{s}$ is the effective area of the collector electrode, and κ is the specific conductivity of the liquid given by

$$\kappa = e_0 \sum_i z_i \mu_i n_i \tag{7}$$

where e_0 is the electron charge, z_i, μ_i, and n_i are the charge number, mobility, and concentration of the ith charged species, respectively.[13]

The experimental results (Figure 3) at room temperature ($T = 296$ K) show a linear dependence between the dark current, i_d, and $n_0 = [(Rb^+,Rb^-)]_{eq} + [Rb^-]_{eq}$, which is the total concentration of Rb^- as free and geminate anions (eq 1). Thus, within the concentration range of n_0 used in our experiments, the dark conductivity of Rb/THF solutions is caused either by Rb^- and Rb^+ and/or other charge carriers generated from the Rb^-, e.g., electrons. For $n_0 \approx 10^{-6}$ kmol m^{-3} the specific conductivity, κ, of the Rb/THF solution is calculated to be 1.8×10^{-5} Ω^{-1} m^{-1}, which is much greater than that of THF, implying that the dark current is a measure of n_0.

In Figure 4, i_d is plotted (line 1) against the inverse temperature for $n_0 = 4.2 \times 10^{-6}$ kmol m^{-3} (blue solution). Line 3 in Figure 4 shows the temperature dependence of the inverse viscosity of THF[14,15]

$$\eta^{-1} = 4680 \exp(-E_a^{(\eta)}/RT) P^{-1} \tag{8}$$

where $E_a^{(\eta)} = 7.5$ kJ mol^{-1} is the activation energy. As seen from Figure 4, the temperature behaviors of i_d and $1/\eta$ are practically the same. This will be discussed below.

III.3. Photoinduced Current. Laser irradiation of Rb/THF solution, while the voltage pulse is on, results in the photoinduced transient current, Δi_p, expressed by

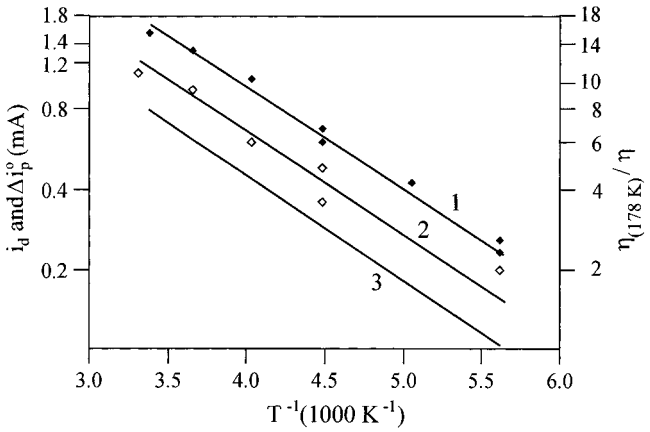

Figure 4. Plots of i_d (1) and Δi_p° (2) vs T^{-1}: $E_0 = 1.53 \times 10^5$ V m^{-1} and $n_0 = 4.2 \times 10^{-6}$ kmol m^{-3}. Lines 1 and 2 are the best-fit lines according to an Arrhenius relation with the same $E_a = 7.1$ kJ mol^{-1}. Line 3 is an Arrhenius plot of $\eta_{(178)}/\eta$ vs T^{-1} with $E_a = 7.5$ kJ mol^{-1}.

$$\Delta i_p = e_0 E_0 A \sum_k \mu_k \Delta n_k \tag{9}$$

where $\Delta n_k = n_k - n_{keq}$, n_k and n_{keq} are the nonequilibrium and equilibrium concentrations, and μ_k is the mobility of kth charged species, respectively. The experimental results shown in Figure 2 can be summarized by several points, which will be treated in detail in the next sections: (1) the photocurrent, Δi_p, consists of a fast component in the range about $t < t_s$ and a slow one in the range of $t > t_s$, where t_s is 1−2 μs. The slow component may last up to 100 μs. (2) The initial amplitude of the fast component, Δi_p°, and the dark current, i_d, decrease upon decreasing [Rb^-], such that the ratio $\Delta i_p^\circ/i_d$ does not depend on [Rb^-] (not shown). A similar behavior of $\Delta i_p^\circ/i_d$ holds for different temperatures (cf. line 1 and 2 in Figure 4). (3) The photoinduced signal attributed to Δi_p occurs only when the electric field is applied and does not depend on the time delay between the voltage and the laser pulses (40−300 μs). (4) Within the time scale of 0.1−1 μs, the decay of the fast component can be approximated into

$$\Delta i_p = (\Delta i_p^\circ - \Delta i_p^s) \exp(-t/\tau_e) + \Delta i_p^s \tag{10}$$

where Δi_p^s is the final quasi-steady-state current in the fast stage, which can be considered as the initial current for the slow component. The decay time, τ_e, was found to increase upon decreasing both the temperature and [Rb^-]. Figure 5a shows how $1/\tau_e$ depends on the dark current, which is a measure of the Rb ions concentration. The temperature dependence of τ_e is presented in Figure 5b and Table 1. (5) Unlike Δi_p°, the amplitude of the slow component, Δi_p^s, decreases with an increase of both the temperature and [Rb^-]. Inspection of Table 1 and Figure 6 shows that by increasing the temperature or [Rb^-], the ratio $\Delta i_p^s/\Delta i_p^\circ$ decreases and passes through zero to negative values (see also Figure 2, iv), where the total detected current, i_p, becomes lower than the dark current level. (6) In all cases, the total current, i_p, approaches, at long times, the initial dark current value, i_d. The time dependence of the slow component ($t > t_s$) shown in Figure 7 could be fitted by the empirical expression

$$\Delta i_p = \Delta i_p^s [1 + (t - t_s)/t_{1/2}]^{-1} \tag{11}$$

where the half-decay time, $t_{1/2}$, was found to increase upon

TABLE 1: Parameters Associated with the Photocurrent and Dark Conductivity Observed at Different Temperatures[a]

	T (K)				
	296	273	248	223	198
ϵ^b	7.49	8.23	9.23	10.43	11.93
τ_e (ns)	290 ± 54	348 ± 87	435 ± 75	580 ± 100	1000 ± 290
u_d (mA)	0.84	0.73	0.565	0.38	0.23
κ (Ω^{-1} m^{-1})	7.4×10^{-5}	6.43×10^{-5}	4.98×10^{-5}	3.35×10^{-5}	2.03×10^{-5}
$4\pi\kappa\tau_e/\epsilon$ (Ω^{-1} cm^{-1} s)	0.32 ± 0.06	0.31 ± 0.08	0.26 ± 0.04	0.21 ± 0.06	0.19 ± 0.06
$\Delta i_p^s/\Delta i_p^\circ$	−0.21 ± 0.04	−0.21 ± 0.03	−0.046 ± 0.015	0.38 ± 0.06	0.75 ± 0.15
χ	2.8 ± 0.6	2.9 ± 0.5	3.2 ± 0.6	3.5 ± 0.6	3.1 ± 0.7
y	0.90 ± 0.04	0.90 ± 0.04	0.85 ± 0.03	0.72 ± 0.03	0.58 ± 0.02
K_3/n_0	0.11	0.11	0.176	0.39	0.72
K_3 (m^{-3} kmol)	4.6×10^{-7}	4.6×10^{-7}	7.4×10^{-7}	16.4×10^{-7}	30.4×10^{-7}
k_{-3} (m^3 kmol^{-1} s^{-1})	7.5×10^{11}	6.2×10^{11}	4.7×10^{11}	2.95×10^{11}	1.4×10^{11}
$\mu_e + \mu_+$ (cm^2 V^{-1} s^{-1})	5.1×10^{-3}	4.6×10^{-3}	3.9×10^{-3}	2.8×10^{-3}	1.5×10^{-3}
μ_e (cm^2 V^{-1} s^{-1})	4.3×10^{-3}	3.9×10^{-3}	3.4×10^{-3}	2.5×10^{-3}	1.3×10^{-3}

[a] For a solution with $n_0 = 4.2 \times 10^{-6}$ m^{-3} kmol. [b] Dielectric constant of THF was calculated as $\epsilon = -1.495 + 2659T^{-1}$.[15]

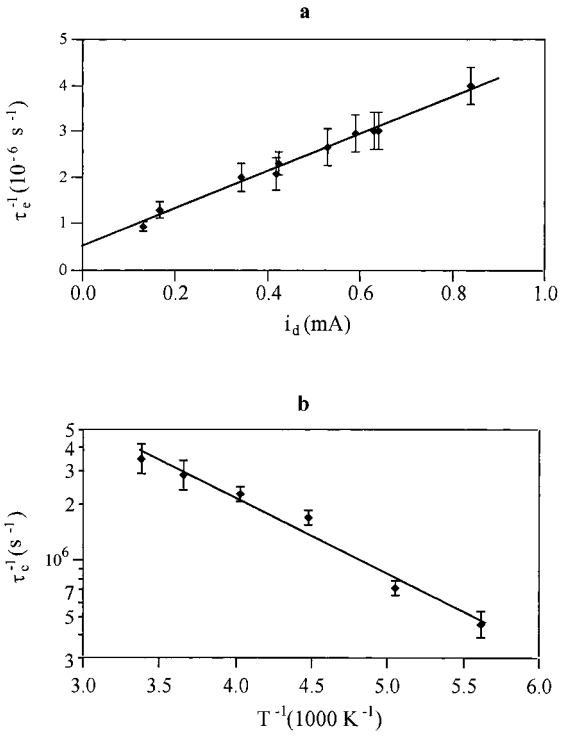

Figure 5. Inverse decay time, τ_e^{-1}, of the fast component of the photocurrent vs dark current, i_d, at $T = 296$ K and $E_0 = 1.53 \times 10^5$ V m^{-1} (a) and as a function of inverse temperature with $n_0 = 4.2 \times 10^{-6}$ kmol m^{-3} (b).

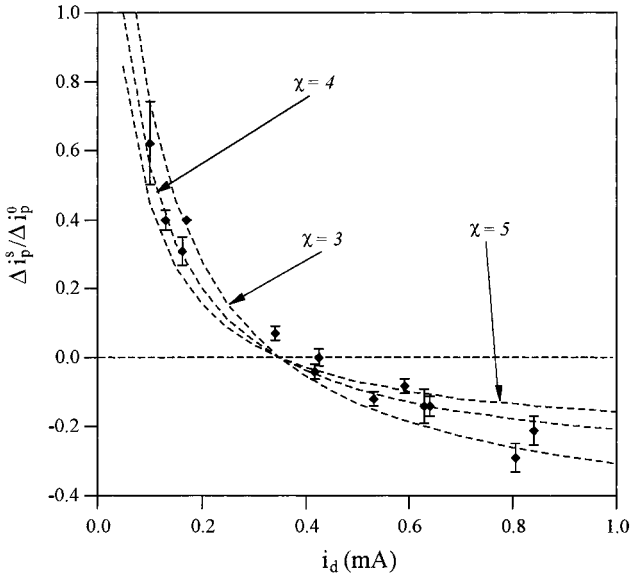

Figure 6. Ratio of the amplitudes of the slow and initial photocurrents vs the dark current: $T = 296$ K and $E_0 = 1.53 \times 10^5$ V m^{-1}. The dashed curves were calculated according to eq 30 with $\chi = 3$, 4, and 5.

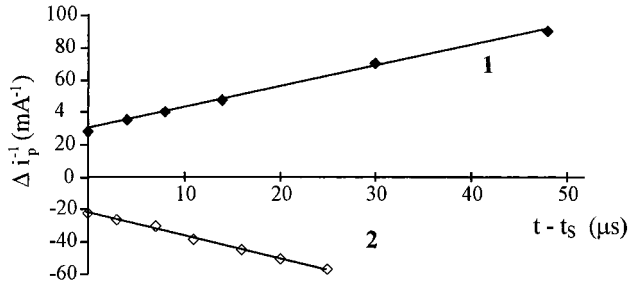

Figure 7. The inverse photocurrent, Δi_p^{-1}, vs $t - t_s$ during the slow stage for $n_0 = 4.2 \times 10^{-6}$ kmol m^{-3}, $W = 7.2$ mJ at (1) $T = 296$ K and (2) $T = 223$ K.

decreasing both the temperature and laser pulse energy, *W*. (7) While $\Delta i_p^\circ/i_d$ does not depend on temperature or [Rb$^-$], we found that it depends linearly on *W* with the slope $\gamma = 30.3 \pm 3.0$ J^{-1} (Figure 8). At typical light pulse energies of 5−10 mJ, the ratio between the initial amplitude of the photocurrent and the dark current level does not exceed 0.1.

IV. Discussion

IV.1. Equilibrium Concentrations of Charge Carriers in Rb/THF Solutions. We consider first the reactions in Rb/THF solutions in the absence of light irradiation. From previous known data, the chemical equilibrium in Rb/THF solutions can be described by the kinetic scheme given by eqs 1−3. Taking into account charge conservation $[Rb^+]_{eq} = [Rb^-]_{eq} + [e^-]_{eq}$, we estimate $[e^-]_{eq}/[Rb^-]_{eq} \le 3 \times 10^{-3}$ for $n_o \approx 4 \times 10^{-6}$ kmol m^{-3}, thus obtaining $[Rb^-]_{eq} \approx [Rb^+]_{eq}$. Although at room temperature the electron mobility (3×10^{-3} cm^2 V^{-1} s^{-1}) is larger than the mobilities of both ions by a factor of 10,[1d,e,8] they do not contribute to the dark conduction because of their low concentration. Thus, the specific conductivity of the Rb/THF solutions is

$$\kappa = e_0[Rb^-]_{eq}(\mu_+ + \mu_-) \qquad (12)$$

where μ_+ and μ_- are the mobilities of the free ions, Rb^+ and Rb^-, respectively. In terms of eq 12 and according to the Stokes law, the temperature dependence of the ion mobility coincides with that of the inverse viscosity, $1/\eta$. As seen from Figure 4,

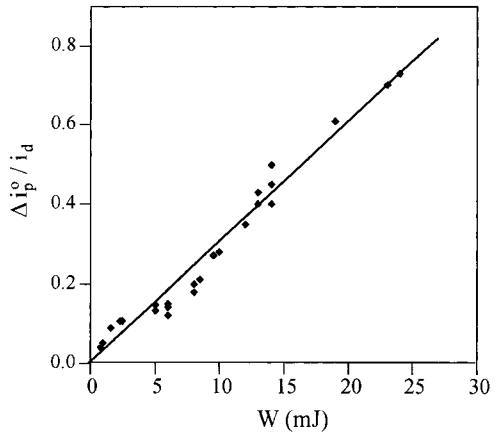

Figure 8. Ratio between the initial photocurrent and the dark current, $\Delta i_p^o/i_d$, vs laser pulse energy, W, at 296 K, with slope $\gamma = 30.3 \pm 3.0$ J^{-1}.

the temperature dependence of the dark current is close to that of $1/\eta$. This implies that the concentrations of Rb^+ and Rb^- do not depend on temperature and that equilibrium 1 is shifted strongly to the right. In other words, most of the Rb ions are not geminate and are free charge carriers.

Such a shift can be confirmed again by estimating the sum of ion mobilities. If all Rb^- ions which contribute to the optical absorption are free, i.e., $[Rb^-]_{eq} = n_0$, then the sum of μ_+ and μ_- can be obtained from the ratio i_d/n_0. It follows from eqs 6 and 12 that at 296 K

$$\mu_+ + \mu_- = \frac{i_d}{n_0}\frac{1}{e_0 E_0 A_{eff}} = (1.6 \pm 0.1) \times 10^{-3}\ \mathrm{cm^2\ V^{-1}\ s^{-1}} \quad (13a)$$

while from the Stokes approximation we have[1e]

$$\mu_+ + \mu_- = \frac{e_0}{6\pi\eta}\left(\frac{1}{r_{Rb^+}} + \frac{1}{r_{Rb^-}}\right) \quad (13b)$$

where r_{Rb^+} and r_{Rb^-} are the corresponding radii. For $\eta = 4.72 \times 10^{-3}$ P at 296 K[14,15] and using eqs 13a and 13b, we calculate $(1/r_{Rb^+} + 1/r_{Rb^-}) = (0.9 \pm 0.07) \times 10^{10}$ m^{-1}. Assuming an equal contribution of cations and anions to the conductivity, we further calculate that $r_{Rb^+} = r_{Rb^-} = 0.225 \pm 0.015$ nm. This value is equal to the Stokes radius of Cs^+.[14] On the other hand, it is known that the equivalent conductivity of the Rb^+ and Cs^+ cations in water are indeed equal at 298 K,[16] and thus, the Stokes radii of Rb^+ and Cs^+ are practically the same, as confirmed by our optical absorption and dark conductivity measurements.

Within experimental error (~10%), the degree of dissociation $\beta = [Rb^-]_{eq}/n_0$ can be approximated to $\beta \approx 1 - n_0/K_1$, where K_1 is the equilibrium constant of reaction 1. For $\beta > 0.9$, it follows that $K_1 > 4 \times 10^{-5}$ kmol m^{-3} at $T = 296$ K.

Within the above findings, it is noteworthy to compare the estimated value of K_1 with that predicted by the Fuoss model[17]

$$K_1 = \frac{3000}{4\pi a_1^{\,3} N_A}\exp\left(-\frac{e_0^{\,2}}{a_1 \epsilon k_B T}\right) \quad (14)$$

where a_1 is the distance of closest approach, N_A is Avogadro's number, ϵ is the dielectric constant, and k_B is Boltzmann's constant. For $K_1 > 4 \times 10^{-5}$ kmol m^{-3} and $\epsilon = 7.49$[15] at 296 K, we obtain that $a_1 > 0.75$ nm. This large distance can be considered as the sum of the Rb^+ and Rb^- radii and at least the diameter of one THF molecule, e.g., $d_{THF} = 0.64$ nm.[18] According to Kruus,[19] the values of the ionic radii, which must be used in liquids, are greater than the crystallographic radius, i.e., about 0.085 nm greater for positive ions and 0.01 nm greater for negative ions. With the crystallographic radius 0.149 nm for Rb^+,[20] we obtain $a_1 = 1.03$ nm for the case of one solvent molecule between ions in the (Rb^+, Rb^-) pair, in line with $a_1 > 0.75$ nm obtained from the Fuoss expression. This reconfirms that the (Rb^+, Rb^-) pair represents a loose ion pair.

Since the dielectric constant of THF increases with cooling according to $d(\ln \epsilon)/d(\ln T) = -1.19$,[15] then according to the Fuoss model (eq 14), K_1 increases as the temperature decreases, as confirmed experimentally for alkali metal salts in THF.[14]

Thus, in the range of 170−296 K, $\beta \approx 1$ and the dark current is proportional to the sum of ion mobilities. From the relation of i_d vs $1/T$ (Figure 4) and eq 13a, the ion mobilities are given by

$$\mu_+ + \mu_- = 0.028 \exp(-E_a^{(d)}/RT)\ \mathrm{cm^2\ V^{-1}\ s^{-1}} \quad (15)$$

where $E_a^{(d)} = 7.1 \pm 1.25$ kJ mol^{-1} is the activation energy of the ion mobilities. On the basis of the results obtained above and reactions 1−3, one may obtain that at equilibrium $[Rb^\bullet]_{eq} < 6 \times 10^{-7}$ kmol m^{-3} and $K_2 < 6 \times 10^{-10}$ kmol m^{-3}.

To summarize this part, we have shown that nonirradiated Rb/THF solutions contain Rb^+ and Rb^- in equal and detectable concentrations. The concentrations of $Rb^\bullet$ and e^- are negligibly small.

IV.2. Kinetic Model of Photoexcited Systems. Qualitatively, the fast component of the photocurrent (Figures 2) is attributed to the photodetached electrons (reaction 4), which recombine with the cations in the back reaction 3.[21S] The "negative photocurrent" at the end of the fast stage at high temperatures and/or high concentrations of the Rb^+ can be attributed to the strong shift of reaction 3 to the left. This implies the temporal reduction of $[Rb^+]$ and $[Rb^-]$ below their equilibrium values. In other words, at the end of the fast stage, the total detected current decreases below the dark current level. According to the Fuoss model, the equilibrium constant K_3 is expected to decrease upon temperature increase, thus shifting this equilibrium to the left and consequently reducing the ion concentrations. The slow component of the photocurrent can be ascribed to slow reactions, namely, to back reaction 2 followed by the annihilation of $Rb^\bullet$ (reaction 5).[12] We now quantitatively discuss the fast and slow processes.

i. Fast Regime. For $t < t_s \approx 2t_{rec}$, where $t_{rec} = (k_{-3}[Rb^+])^{-1}$ is the characteristic time of recombination, slow reactions 2 and 5 are neglected. Thus, the concentrations of e^-, Rb^-, and Rb^+ are obtained by solving the two equations

$$d[e^-]/dt = d[Rb^+]/dt = -k_{-3}[e^-][Rb^+] + k_3[Rb^\bullet] \quad (16)$$

$$d[Rb^\bullet]/dt = k_{-3}[e^-][Rb^+] - k_3[Rb^\bullet] \quad (17)$$

with the initial conditions $[Rb^+] = n_0$ and $[e^-] = [Rb^\bullet] = [e^-]_0$ ($[e^-]_0$ is the initial concentration of photodetached electrons). From eqs 16 and 17, $[e^-] + [Rb^\bullet] = 2[e^-]_0$. In our case, where light intensities are low, $[e^-]_0 \ll n_0$ and $[Rb^+] \approx n_0$. Under such conditions, the temporal behaviors of the different species are expressed by

$$[e^-] = [e^-]_0 \left\{ \frac{2K_3}{n_0 + K_3} + \frac{n_0 - K_3}{n_0 + K_3} \exp(-t/\tau_e) \right\} \quad (18)$$

$$[Rb^\bullet] = 2[e^-]_0 - [e^-] = [e^-]_0 \left\{ \frac{2n_0}{n_0 + K_3} - \frac{n_0 - K_3}{n_0 + K_3} \exp(-t/\tau_e) \right\} \quad (19)$$

$$[Rb^+] = n_0 - [e^-]_0 + [e^-] \quad (20)$$

$$[Rb^-] = n_0 - [e^-]_0 \quad (21)$$

where $1/\tau_e = k_{-3}n_0 + k_3$. According to eq 9, the photoinduced current is expressed by

$$\Delta i_p = e_0 E_0 A\{\mu_e[e^-] + \mu_+([Rb^+] - n_0) + \mu_-([Rb^-] - n_0)\} \quad (22)$$

At $t = 0$, eq 22 becomes $\Delta i_p^\circ = e_0 E_0 A[e^-]_0(\mu_e - \mu_-)$, and at $t = \infty$, it approaches the asymptotic form $\Delta i_p^s = e_0 E_0 A[e^-]_0 [(2\mu_e + \mu_+ - \mu_-)K_3 - (\mu_+ + \mu_-)n_0]/(n_0 + K_3)$, which serves as the initial amplitude for the slow component. The sign of Δi_p^s depends upon the relationship between $(2\mu_e + \mu_+ - \mu_-)K_3$ and $(\mu_+ + \mu_-)n_0$. Thus, the empirical eq 10 is fully consistent with that derived through eqs 16 and 17.

ii. Slow Regime. To account for the slow decay of the photocurrent (at $t > t_s$), we consider back reaction 2 and the processes described by reactions 3 and 5. Under such conditions, the concentration of electrons, which is the most reactive species, is considered to be quasi-stationary. The following coupled equations should be considered

$$\frac{d}{dt}[e^-] = -k_{-3}[e^-][Rb^+] + k_3[Rb^\bullet] + k_{-2}[e^-][Rb^\bullet] = 0 \quad (23)$$

$$\frac{d}{dt}[Rb^\bullet] = k_{-3}[e^-][Rb^+] - k_3[Rb^\bullet] - k_{-2}[e^-][Rb^\bullet] - 2k_5[Rb^\bullet]^2 \quad (24)$$

$$\frac{d}{dt}[Rb^+] = k_3[Rb^\bullet] - k_{-3}[e^-][Rb^+] + k_5[Rb^\bullet]^2 \quad (25)$$

$$\frac{d}{dt}[Rb^-] = k_{-2}[e^-][Rb^\bullet] + k_5[Rb^\bullet]^2 \quad (26)$$

with the initial conditions (at $t = t_s$) $[Rb^-]_s = n_0 - [e^-]_0$, $[Rb^+]_s = n_0 - [e^-]_0(n_0 - K_3)/(n_0 + K_3)$, $[e^-]_s = 2[e^-]_0K_3/(n_0 + K_3)$, and $[Rb^\bullet]_s = 2[e^-]_0n_0/(n_0 + K_3)$, where subscript s stands for concentrations at $t = t_s$, which corresponds to the asymptotic limits of eqs 18−21.

For $k_3 \gg k_{-2}[e^-]$, from eq 23 we obtain that at $t > t_s$, $[e^-] \approx K_3[Rb^\bullet]/n_0$. The decay of $Rb^\bullet$ is given by

$$[Rb^\bullet] = [Rb^\bullet]_s[1 + (t - t_s)/t_{1/2}]^{-1} \quad (27)$$

with $t_{1/2} = [4[e^-]_0(k_{-2}K_3 + k_5n_0)/(n_0 + K_3)]^{-1}$. Adding together eqs 24−26 we obtain

$$\frac{d}{dt}([Rb^+] + [Rb^\bullet] + [Rb^-]) = 0 \quad (28)$$

In terms of eqs 22, 27, and 28 with the approximation that $\mu_+ = \mu_- = \mu_{ion}$,[1e] the initial amplitude of the photocurrent slow component is

$$\Delta i_p^s = \frac{2[e^-]_0}{n_0 + K_3}(\mu_e K_3 - \mu_{ion} n_0) \quad (29)$$

IV.4. Reaction Rates and Mobility. On the basis of the model and experimental results discussed above, we can obtain the different rate constants, equilibrium constants, mobilities, and their temperature dependences.

i. Room Temperature. Combining the experimental results of Figure 5a and the expression for $1/\tau_e$ (cf. eqs 18 and 19) with $n_0/i_d = 4.86 \times 10^{-6}$ kmol m^{-3} mA^{-1} (Figure 3), we obtain that at 296 K $k_{-3} = (8.2 \pm 1.5) \times 10^{11}$ m^3 kmol^{-1} s^{-1}. The value of K_3 can be determined from the experimental dependence of the ratio $\Delta i_p^s/\Delta i_p^\circ$ vs the dark current shown in Figure 6. Using the expressions of Δi_p° and Δi_p^s (derived from eq 22) the ratio of the initial slow and fast currents is given by

$$\frac{\Delta i_p^s}{\Delta i_p^\circ} = \left(\frac{K_3}{n_0 + K_3}\right)\left(\frac{2\chi}{\chi - 1}\right) - \left(\frac{1}{\chi - 1}\right) \quad (30)$$

where $\chi = (\mu_e + \mu_+)/(\mu_+ + \mu_-)$. From eq 30 and Figure 6 it follows that at a certain initial ion concentration, n_0^*, $\Delta i_p^s/\Delta i_p^\circ = 0$ and under such conditions K_3 can be expressed as

$$K_3 = n_0^*/(2\chi - 1) \quad (31)$$

The dashed lines in Figure 6 are the simulations based on eq 30 with $n_0^* = 1.75 \times 10^{-6}$ kmol m^{-3}, which corresponds to $i_d = 0.35$ mA, and $\chi = 3$, 4, and 5, from which K_3 is calculated to be $(2.5 \pm 1.0) \times 10^{-7}$ kmol m^{-3}. Since $\mu_+ = \mu_- = (8.0 \pm 1.0) \times 10^{-4}$ cm^2 V^{-1} s^{-1}, we obtain also that $\mu_e = (5.4 \pm 1.35) \times 10^{-3}$ cm^2 V^{-1} s^{-1}.

The electron mobility can be also estimated from the value of k_{-3} obtained above assuming that the electron recombination in THF obeys the Debye−Langevin equation[22]

$$k_{-3} = 4\pi e_0(\mu_e + \mu_+)/\epsilon \quad (32)$$

Using $\epsilon = 7.49$[15] and the values of μ_+ and k_{-3}, we calculate that $\mu_e = 5.3 \times 10^{-3}$ cm^2 V^{-1} s^{-1}, which almost coincides with the value obtained from Figure 6.

By combining eqs 6 and 7 with the expression for Δi_p°, the cross-section (σ_p) of the electron photodetachment from Rb^- is given by

$$\sigma_p = \frac{\Delta i_p^\circ}{i_d} \frac{E_\nu A_{eff} S}{(\chi - 1)AW} \quad (33)$$

where E_ν (2.33 eV) is the photon energy at 532 nm, $W/E_\nu S$ is the photon flux density (Φ) during the laser pulse (in photons/m^2), and $S = 9 \times 10^{-6}$ m^2 is the area of the diaphragm (13 in Figure 1). Here, we also took into account that for $\Phi\sigma_p \ll 1$, an initial concentration of photoelectrons generated by the laser pulse is $[e^-]_0 = \Phi\sigma_p n_0$. Taking into account eqs 33 and $\chi = 4$ (Figure 6), we obtain that $\sigma_p \approx 0.8 \times 10^{-22}$ m^2. This value is much smaller than the absorption cross section of Rb^- in THF at 532 nm, i.e., $\sigma_a = 1.9 \times 10^{-21}$ m^2, found from the extinction coefficient of Rb^-.[9] The low quantum yield of electron photodetachment, i.e., $\sigma_p/\sigma_a \approx 0.04$, is possibly due to the low probability for the photodetached electron to escape back reaction with its geminate $Rb^\bullet$. For typical laser energies of $W = 5$ mJ, the fraction of Rb^- converted to electrons during the laser pulse is small, ($[e^-]_0/n_0 = \Phi\sigma_p \approx 0.1$). This confirms the assumption of low electron concentrations.

ii. Temperature Dependence. It was shown that Δi_p° is proportional to the product $\sigma_p(\mu_e - \mu_-)$. The temperature dependence of μ_e can be found only if the temperature dependence of σ_p is known. Unfortunately, a temperature behavior of σ_p for the Rb^- anions has not been investigated yet. It is known that the electron photodetachment from a number of molecular anions in polar solvents, like the ferricyanide ion in water, is a single-photon thermally-activated process, i.e., σ_p should depend on the temperature.[23] Therefore, to avoid any assumptions on the temperature dependence of σ_p, we utilize a different approach based on the experimental decay times of the fast photocurrent and the Debye−Langevin expression (eq 32) for the electron recombination rate. Using eqs 32 and 7 and the expression for $1/\tau_e$, we obtain

$$y = n_0/(n_0 + K_3) = (4\pi\kappa\tau_e/\epsilon)\chi \tag{34}$$

From the expressions for Δi_p° and Δi_p^s (cf. eq 22) it follows that

$$y = 1 - \frac{\Delta i_p^{\,s}}{2\Delta i_p^\circ} - \frac{(1 - \Delta i_p^{\,s}/\Delta i_p^\circ)}{2\chi} \tag{35}$$

Solving eqs 34 and 35 numerically results in K_3, and from the expression for $1/\tau_e$ (cf. eqs 18 and 19) and eq 32, k_{-3} and μ_e can be obtained. The results at different temperatures are summarized in Table 1. The dielectric constant of THF was calculated through the relation $\epsilon = -1.495 + 2659/T$.[15]

It is noteworthy that K_3 values at room temperature obtained through different approaches are the same within the experimental error. The results for μ_e and k_{-3} in Table 1 obey the relations (Figure 9S)

$$\mu_e = (5.2 \pm 2.7) \times 10^{-2} \exp(-E_a^{(e)}/RT)\ \mathrm{cm^2\ V^{-1}\ s^{-1}} \tag{36}$$

$$k_{-3} = (2.4 \pm 0.9) \times 10^{13} \exp(-E_a^{(-3)}/RT)\ \mathrm{kmol^{-1}\ m^3\ s^{-1}} \tag{37}$$

where $E_a^{(e)} = 5.9 \pm 1.0$ kJ mol^{-1} and $E_a^{(-3)} = 8.4 \pm 0.4$ kJ mol^{-1} are the activation energies. The value of $E_a^{(e)}$ is below the activation energy of 9−14 kJ mol^{-1} observed in other ethers at low temperatures.[8] It is also below the activation energy of η^{-1} calculated from Figure 4, i.e., $E_a^{(\eta)} = 7.5$ kJ mol^{-1}. This relatively low value of $E_a^{(e)}$ is interpreted by the trapping model, where the mobility is associated with the electron hopping between a quasi-free state with a mobility $\mu_e^{(f)}$ and lifetime τ_f and a localized (trapped) state with mobility $\mu_e^{(l)}$ and a lifetime τ_1.[24] Thus, an expression for the apparent mobility is defined as[4]

$$\mu_e = \frac{\tau_1}{\tau_1 + \tau_f}\mu_e^{(1)} + \frac{\tau_f}{\tau_1 + \tau_f}\mu_e^{(f)} \tag{38}$$

Assuming that $\tau_1 \gg \tau_f$ one obtains

$$\mu_e = \mu_e^{(1)} + \frac{\tau_f}{\tau_1}\mu_e^{(f)} \tag{39}$$

Indeed, experimental data show that a conduction band exists in ethers.[8,25] To simulate the temperature dependence of μ_e, we have taken into account that (1) the mobility of the localized state is ion-like with an activation energy $E_a^{(\eta)} = 7.5$ kJ mol^{-1} (eq 8); (2) $\tau_f/\tau_1 = \exp(-E_a^{cb}/RT)$, where E_a^{cb} is the thermal energy barrier between the electron energy level and the solvent conduction band; and (3) $\mu_e^{(f)} \approx 100$ cm^2 V^{-1} s^{-1}.[1b,22c,25] Within these assumptions the experimental data shown in Figure 9aS could be fitted with the expression

$$\mu_e = A \exp\left(-\frac{900}{T}\right) + 100 \exp\left(-\frac{B}{T}\right)\ \mathrm{cm^2\ V^{-1}\ s^{-1}} \tag{40}$$

with the best-fit parameters $A = 0.15$ cm^2 V^{-1} s^{-1} and $B = 3500$ K.

A very similar expression, for modeling electron mobility in various ethers was used by Dodelet and Freeman.[8] They also measured μ_e in THF at room temperature and obtained a value of 0.003 cm^2 V^{-1} s^{-1}, which is somewhat smaller than our value. However, taking into account different methods of electron production, the agreement is satisfactory. The value of 30 kJ mol^{-1} obtained for E_a^{cb} is in line with the optical absorption spectrum of e^- in THF, which has been attributed to the bound-to-continuum transition.[1e,26] The low-energy Gaussian tail of the absorption band correlates with the value of E_a^{cb}.

Finally, the best fit of the equilibrium constant K_3 in its Arrhenius form $K_3 = A_3 \exp(E_a^{(3)}/RT)$ is shown in Figure 9cS, where $A_3 = (6.1 \pm 2.6) \times 10^{-9}$ kmol m^{-3} and $E_a^{(3)} = 10.0 \pm 0.6$ kJ mol^{-1}.[27]

We can now estimate the temperature dependence of the photodetachment cross section, σ_p. Since $(\mu_e - \mu_-)$ and $(\mu_+ + \mu_-)$ are characterized by activation energies $E_a^{(e)} = 5.9 \pm 1.0$ kJ mol^{-1} and $E_a^{(d)} = 7.1 \pm 1.25$ kJ mol^{-1}, respectively, it follows from eq 35 that σ_p has a low activation energy of $(E_a^{(d)} - E_a^{(e)}) = 1.25 \pm 1.25$ kJ mol^{-1}.

IV.5. Electron Attachment to the Rb Atom and Rb−Rb Annihilation. We now discuss the mechanisms of back reaction 2 and annihilation reaction 5. We assume that both reactions are diffusion-controlled, with rate constant given by

$$k_{-2} = 4\pi a_2(D_{e^-} + D_{Rb\bullet}) \tag{41}$$

$$k_5 = 4\pi a_5(D_{Rb\bullet} + D_{Rb\bullet}) \tag{42}$$

where a_2 and a_5 are typical reaction radii ($a_2 = a_5 = 5$ nm) and D_{e^-} and $D_{Rb\bullet}$ are the diffusion coefficients of e^- and $Rb\bullet$ species, respectively. In addition, to a first approximation, a_2 and a_5 are assumed to be temperature independent and $D_{Rb\bullet}$ coincides with the diffusion coefficient of the cation Rb^+ (D_+). Since $D_e = \mu_e k_B T/e_0$ and $D_+ = \mu_+ k_B T/e_0$, they are proportional to the product of temperature and current. The temperature dependence of the rate constants can be obtained from the temperature dependencies of $(\mu_+ + \mu_-)$ and i_d by the following expressions

$$k_{-2}(T) = k_{-2}(296)\frac{(\mu_e + \mu_+)_T}{(\mu_e + \mu_+)_{296}}\frac{T}{296} \tag{43}$$

$$k_5(T) = k_5(296)\frac{i_d(T)}{i_d(296)}\frac{T}{296} \tag{44}$$

Inserting eqs 43 and 44 into the expression for $t_{1/2}$ (eq 27) results in the lifetime and temperature dependence of the slow component of the photocurrent (Table 2S). Except for low temperatures, the calculated values of $t_{1/2}$ and those extracted directly from the kinetic curves are in good agreement. The disagreement at 198 K (Table 2S) is attributed to the fact that the diffusion approximation is not valid at low temperatures.

V. Summary

To summarize, reactions 1−5 describe the overall kinetics spanning a wide time regime. It should be noted that the annihilation process (reaction 5) is essential to explain the

observed decay times of the slow component of the photocurrent. Actually, when $k_5 = 0$, a comparison between the calculated and the experimental value of $t_{1/2}$ at room temperature results in a very high rate constant, $k_{-2} = 2 \times 10^{11}$ m^3 kmol^{-1} s^{-1}, corresponding to an extremely large and unrealistic reaction radius, $a_2 \approx 3$ nm. It is gratifying that the electron mobility of 1×10^{-3} cm^2 V^{-1} s^{-1} (at 180 K) obtained in this work is in a good agreement with the recalculated value of μ_e (2.5×10^{-3} cm^2 V^{-1} s^{-1}) based upon EPR measurements[3] and the kinetic parameters obtained in this work.

Acknowledgment. This work was supported by Grants of the Israel Ministry of Infrastructure and the Israel Science Foundation (H.L.) and Giladi Foundation (V.R.). The visit of L.L. was supported by the Hebrew University of Jerusalem. This work is in partial fulfillment of the requirements for a Ph.D. degree (Y.H.) at the Hebrew University of Jerusalem. L.L. is supported by Grant No. 97-03-32018 of the Russian Basic Research Foundation.

Supporting Information Available: Ref 21S, Figure 9S, and Table 2S. This material is available free of charge via the Internet at http://pubs.acs.org.

References and Notes

(1) (a) Feng, D.-F.; Kevan, L. *Chem. Rev.* **1980**, *80*, 1. (b) Yakovlev, B. S.; Lukin, L. V. *Adv. Chem. Phys.* **1985**, *60*, 99. (c) Brodskii, A. M.; Tsarevskii, A. V. *Russ. Chem. Rev.* **1987**, *56*, 969. (d) Schmidt, W. F. *Liquid State Electronics of Insulating Liquids*; CRC Press: New York, 1997. (e) Pikaev, A. K. *Modern Radiation Chemistry*; Nauka: Moscow, 1986.

(2) Johnson, M. *Science* **1993**, *260*, 320.

(3) Rozenshtein, V.; Heimlich, Y.; Levanon, H. *J. Phys. Chem. A* **1997**, *101*, 3197.

(4) Schmidt, W. F. *Can. J. Chem.* **1977**, *55*, 2197.

(5) (a) Dye, J. L. *Pure Appl. Chem.* **1977**, *49*, 3. (b) Dye, J. L. In *Progress in Inorganic Chemistry*; Lippard, S. J., Ed.; Wiley: New York, 1984; Vol. 32, pp 327−441.

(6) (a) Freeman, G. R. In *Kinetics of Nonhomogeneous Processes*; Freeman, G. R., Ed.; Wiley: New York, 1987; Chapter 2. (b) Freeman, G. R. In *The Liquid State and Its Electrical Properties*; Kunhardt, E. E., Christophorou, L. G., Luessen, L. H., Eds.; Plenum: New York, 1988; pp 251−272.

(7) (a) Eliav, U.; Levanon, H.; Carton, P. M.; Fessenden, R. W. *Chem. Phys. Lett.* **1981**, *82*, 365. (b) Rozenshtein, V.; Zilber, G.; Rabinovitz, M.; Levanon, H. *J. Am. Chem. Soc.* **1993**, *115*, 5193. (c) Rozenshtein, V.; Zilber, G.; Levanon, H. *J. Phys. Chem. A* **1994**, *98*, 4236.

(8) Dodelet, J. P.; Freeman, G. R. *Can. J. Chem.* **1975**, *53*, 1263.

(9) (a) Seddon, W. A.; Fletcher, J. W.; Sopchyshyn, F. C.; Selkirk, E. B. *Can. J. Chem.* **1979**, *57*, 1792. (b) Seddon, W. A.; Fletcher, J. W. *Phys. Chem.* **1980**, *84*, 1104.

(10) Glarum, S. H.; Marshall, J. H. *J. Chem. Phys.* **1970**, *52*, 5555.

(11) Fletcher, J. W.; Seddon, W. A.; Sopchyshyn, F. C. *Can. J. Chem.* **1973**, *51*, 2975.

(12) Salmon, G. A.; Seddon, W. A.; Fletcher, J. W. *Can. J. Chem.* **1974**, *52*, 3259.

(13) The effective area of the electrode was obtained by measuring the conductivity of an aqueous solution of NaCl in the same photoelectric cell, resulting in $\alpha = A_{ef}/A = 2.7 \pm 0.1$.

(14) Carvajal, C.; Tolle, K. J.; Smid, J.; Szwarc, M. *J. Am. Chem. Soc.* **1965**, *87*, 5548.

(15) Metz, D. J.; Glines, A. *Phys. Chem.* **1967**, *71*, 1158.

(16) Moelwyn-Hughes, E. A. *Physical Chemistry*, 2nd ed.; Pergamon Press: New York, 1961.

(17) Fuoss, R. M. *J. Am. Chem. Soc.* **1958**, *80*, 5059.

(18) Marcus, Y. *Ion Solvation*; Wiley: Chichester, 1985.

(19) Kruus, P. *Liquids and Solutions Structure and Dynamics*; Marcel Dekker: New York, 1977.

(20) Efimof, B. *Handbook of Inorganic Compounds*; Chimia: Moscow, 1983.

(21) Effect of impurities is negligible, see Supporting Information 21S.

(22) (a) Debye, P. *Trans. Electrochem. Soc.* **1942**, *82*, 265. (b) Hummel, A. *Adv. Rad. Chem.* **1974**, *1*, 1. (c) Yakovlev, B. S. *Russ. Chem. Rev.* **1979**, *48*, 615.

(23) (a) Stein, G. *Adv. Chem. Ser.* **1965**, *50*, 230. (b) Shirom, M.; Stein, G. *J. Chem. Phys.* **1971**, *55*, 3372.

(24) (a) Minday, R. M.; Schmidt, L. D.; Davis, H. T. *J. Chem. Phys.* **1971**, *54*, 3112. (b) Munoz, R. C. In *Excess Electrons in Dielectric Media*; Ferradini, C., Jay-Gerin, Y. P., Eds.; CRC Press: Boca Raton, FL, 1985; pp 161−210.

(25) Holroyd, R. A.; Itoh, M.; Nishikawa, M. *Chem. Phys. Lett.* **1997**, *266*, 227.

(26) Dye, J. L. In *Electrons in Fluids*; Jortner, J., Kestner, N. R., Eds.; Springer-Verlag: Berlin, 1973; p 77.

(27) $E_a^{(3)}$ can be derived from eq 14, with the assumption that the distance of closest approach a_3 in eq 3 is temperature dependent:

$$E_a^{(3)} = k_B \frac{d(\ln K_{-3})}{d(T^{-1})} = -\frac{e_0^2}{\epsilon a_3}\left[1 + \frac{d(\ln \epsilon)}{d(\ln T)}\right] - \frac{k_B T^2 (r_c/a_3 - 3) d(a_3)/dT}{a_3}$$

where $r_c = e^2/\epsilon k_B T$ is the Onsager radius. With $\epsilon = 7.49$ (296 K), $d(\ln \epsilon)/d(\ln T) = -1.16$,[15] $a_3 = 0.469$ nm (296 K), $E_a^{(3)} = 10$ kJ mol^{-1}, we have $da_3/dT = -1.61 \times 10^{-2}$ nm K^{-1}.